Electronic Supplementary Information (ESI)

Tunable Electrochromic Behavior in Titanium-based MXenes

Geetha Valurouthu, Kathleen Maleski, Narendra Kurra, Meikang Han, Kanit Hantanasirisakul, Asia Sarycheva and Yury Gogotsi*

A. J. Drexel Nanomaterials Institute and Department of Materials Science and Engineering, Drexel University, Philadelphia, PA 19104, USA

E-mail: gogotsi@drexel.edu

Procuring of parental MAX phases

Ti_3AlC_2

Layered ternary carbide Ti_3AlC_2 (MAX phase) powder was produced by Carbon-Ukraine, Ltd, with particle size < 40 µm.

Ti_3AlCN

Ti_3AlCN MAX powder was prepared following a procedure reported elsewhere.[S1] Briefly, elemental Ti (Alfa Aesar, 99.5 wt.% purity), AlN (Sigma-Aldrich, 99 wt.% purity), and graphite (Alfa Aesar, 99 wt.% purity; particle size < 48 µm) with a molar ratio of 3:1:1 were ball-milled for 18 h in a plastic jar with 10 mm-diameter zirconia milling balls at 50 rpm. The powder mixture was heated under Ar flow (100 mL/min) in a tube furnace at 1500 °C (at a heating rate of 10 °C/min) and held for 2 h. After cooling down to room temperature, the resulting block of Ti_3AlCN MAX was crushed via drill-milling and sieved through a 400-mesh sieve (particle size < 38 µm).

Ti_2AlC

Ti_2AlC MAX was synthesized by ball-milling TiC (particle size ~2 µm, Ti (particle size <44 µm) and Al (particle size < 44 µm) for 18 h using zirconia balls in plastic jars. The TiC:Ti:Al ratio was 0.9:1.1:1.1. The powder mixture was heated in an alumina crucible at 5 °C/min to 1300 °C and held for 2 h under flowing Argon. After cooling to room temperature, the block of Ti_2AlC MAX was crushed via drill-milling and sieved through a 400-mesh sieve (particle size < 38 µm).

$Ti_{1.6}Nb_{0.4}AlC$

Initially, the precursor powders, Nb, Ti, Al, and graphite were mixed with the atomic ratios of 0.4:1.6:1.1:0.9. The powder mixture was placed into ceramic crucibles and into a Carbolite furnace. The furnace was heated at 3 °C/min to 1550 °C and maintained for 2 h followed by cooling to room temperature at the same rate. The powders were ground in a mortar and sieved through a 400-mesh sieve (particle size < 38 µm).

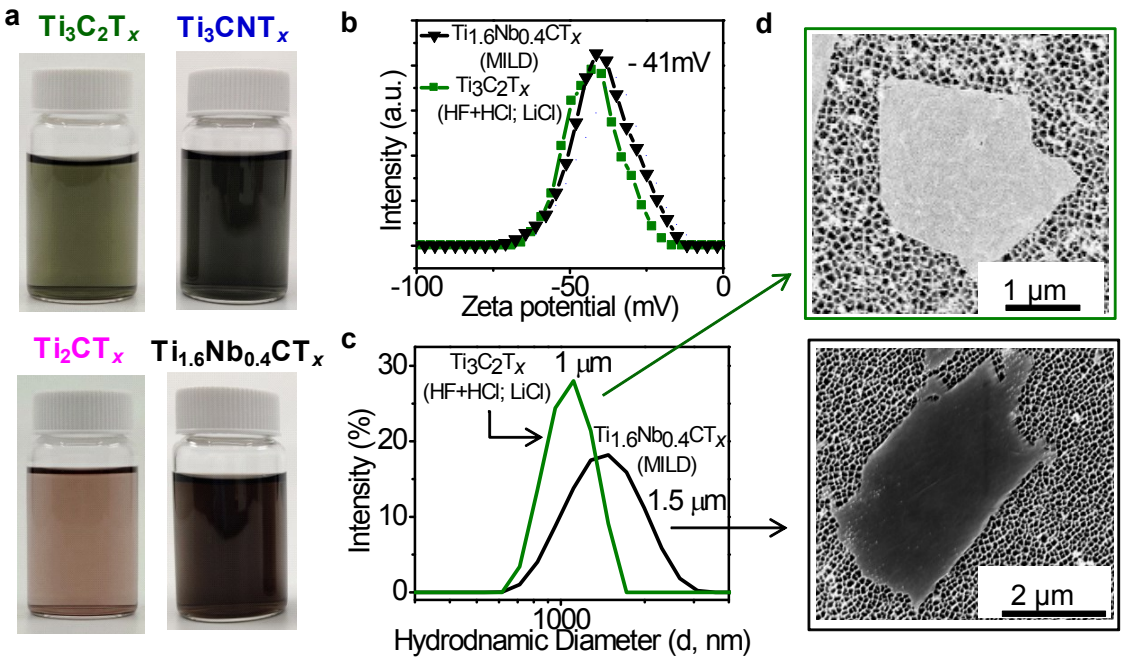

Fig. S1 (a) Digital images of titanium-based MXene colloidal solutions, $Ti_3C_2T_x$, Ti_3CNT_x, Ti_2CT_x, and $Ti_{1.6}Nb_{0.4}CT_x$, in 20 mL glass vials. (b) Static zeta potential intensity distribution (%) at neutral pH. (c) Dynamic light scattering particle size analysis showing the intensity distribution (%). (d) SEM micrographs showing flakes of $Ti_3C_2T_x$, and $Ti_{1.6}Nb_{0.4}CT_x$.

The zeta potential and particle size of the colloids were estimated using dynamic light scattering (DLS) and were performed by pipetting 1 mL of diluted colloid solution into a polystyrene cuvette or dip-cell capillary cuvette (Zetasizer Nano ZS, Malvern Instruments, USA). MXene colloids of different compositions can be visually differentiated as shown in Fig. S1a. DLS average was taken over a total of five measurements from each colloidal sample. As two different protocols were followed to prepare different MXenes, DLS measurements were taken for $Ti_3C_2T_x$ and $Ti_{1.6}Nb_{0.4}CT_x$ prepared by different methods as a representation (Fig. S1b, c). The surface functional groups (=O, -F, -OH, -Cl) obtained from the etching and delamination of MAX, impart negative zeta potential of 41 mV at a neutral pH of 6-7 presented in Fig. S1b offering stable dispersions in water without additional surfactants. Typical average flake sizes were estimated to be ~ 1 µm (Fig. S1c) using DLS and confirmed by the SEM images obtained for the respective MXenes (Fig. S1d).

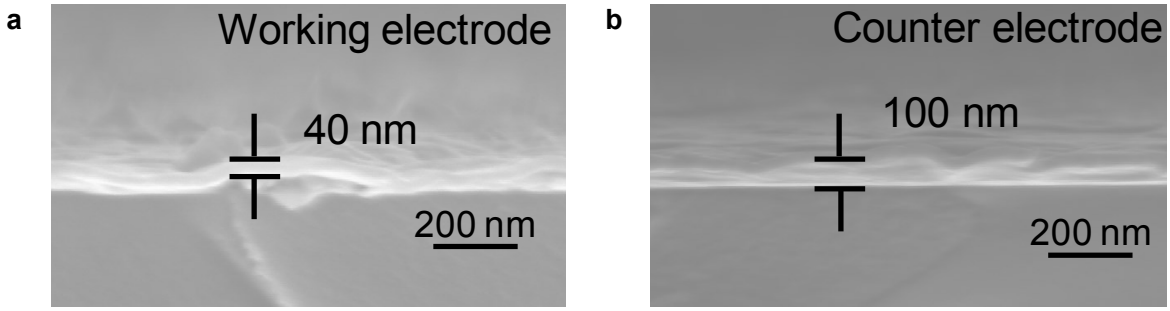

Fig. S2 SEM cross-sectional view of spray-coated (a) working and (b) counter electrodes, typical thicknesses of corresponding films are marked.

To have a rough estimation of the spray-coated film thickness used in the electrochromic devices, cross-section SEM is performed. Fig. S2a and b show the SEM cross-section view of the MXene thin films used as working electrode and counter electrode. The thicknesses were roughly estimated to be 40 and 100 nm, respectively.

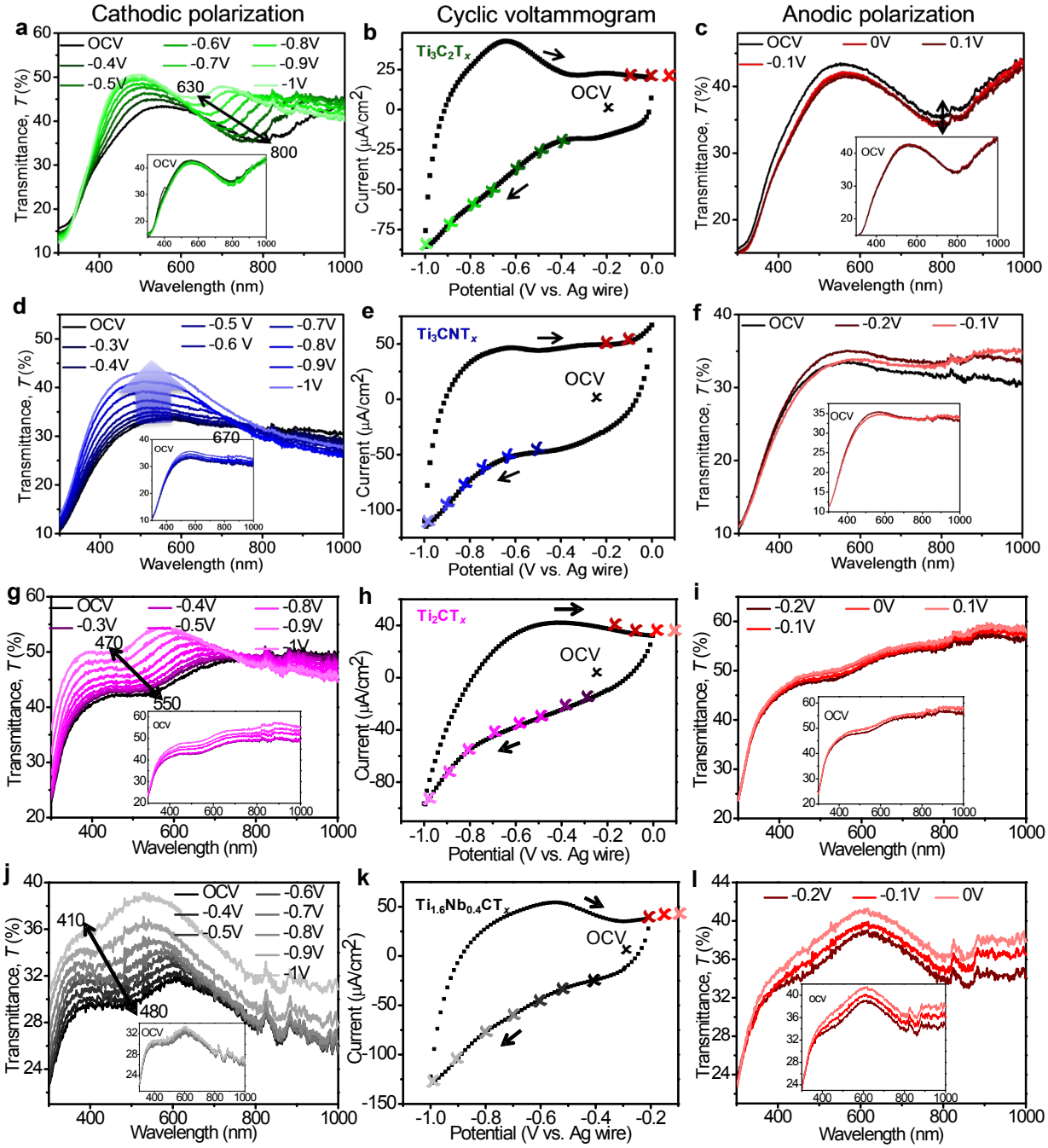

Fig. S3 In-situ opto-electrochemical behavior of $Ti_3C_2T_x$, Ti_3CNT_x, Ti_2CT_x, and $Ti_{1.6}Nb_{0.4}CT_x$ thin films. (a), (d), (g) and (j) extinction spectral shift upon cathodic polarization (chronoamperometry, square pulse applied for 10 min) of MXene thin film electrodes. (b), (e), (h) and (k) CV profiles of electrochromic devices at 20 mV/s. Extinction spectra (c), (f), (i) and (l)

upon anodic polarization. Insets showing the retrace of UV-vis spectra to same spectrum as OCV condition after relaxation from each potential polarization step.

When the MXene thin films were polarized to anodic potentials (E_{anodic} > OCV), there was no significant change in the extinction spectra (Fig. S3c, f, i and l). This is due to capacitive type double layer (de)sorption of ions without change of Ti-redox state. These results again support that Ti-redox state change is responsible for the tunable optical properties of MXene thin films. It is important to note that there were no changes in the transmittance of MXene thin films during anodic polarization (only up to stable potential limit). The inset shows the reversibility of optical properties when the device is allowed to relax after the application of potential (square pulse). Areal discharge capacitance is calculated using the following equation,

$$Areal\ Discharge\ Capacitance = \frac{1}{VA\nu}\int i \times dV \quad \ldots \text{ equation E1}$$

where $\int i \times dV$ is the integrated area of the discharge portion of the cyclic voltammogram (i being current in mA and V being potential), A is area (cm^2) of the working electrode in contact with electrolyte, V is potential window of electrode material, and ν is scan rate (mV/s) with which potential is swept.

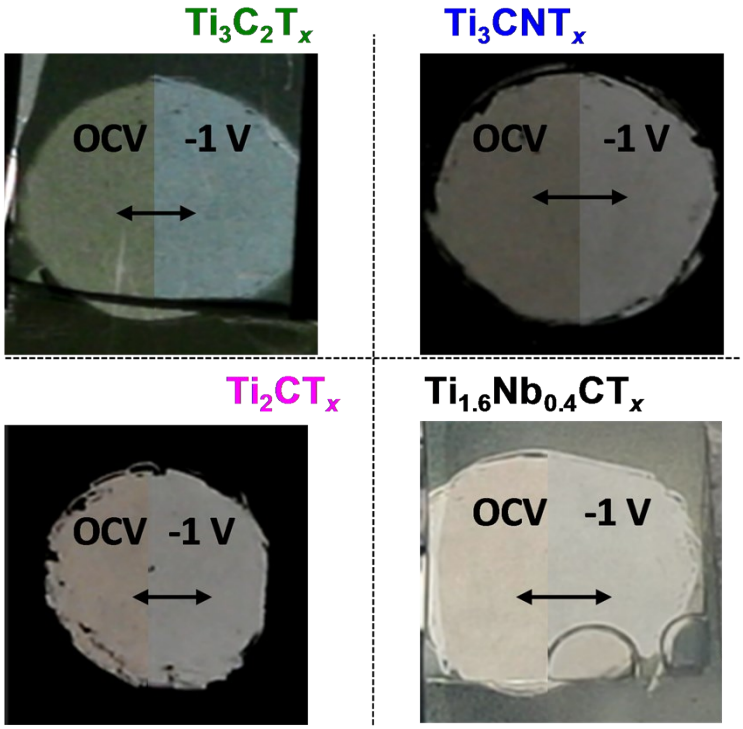

Fig. S4 Digital photographs of MXene thin films under applied cathodic potential (-1 V vs. Ag wire) and OCV. $Ti_3C_2T_x$ showing the color change from Pale green (OCV) to light blue (-1 V), similarly Ti_3CNT_x, Ti_2CT_x, and $Ti_{1.6}Nb_{0.4}CT_x$ showing a change in contrast from darker to lighter tone.

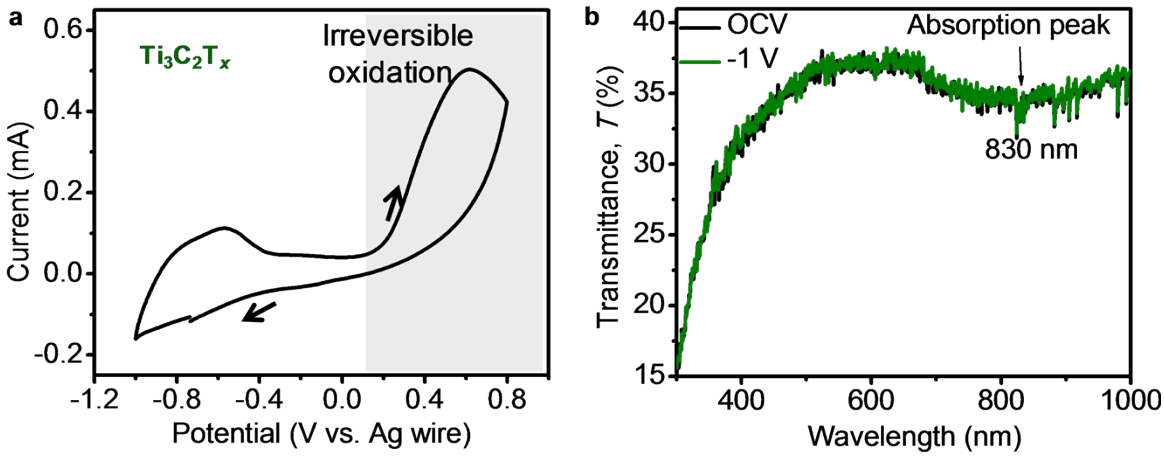

Fig. S5 (a) CV of $Ti_3C_2T_x$ under cathodic and anodic potentials. At high anodic potential (0.8 V vs. Ag wire), irreversible oxidation was observed. (b) UV-vis spectra showing no change of optical extinction peak for oxidized MXene even during cathodic polarization (at -1 V vs. Ag wire).

To confirm the reversible color change is due to change of redox state of Ti, we have anodically oxidized $Ti_3C_2T_x$ thin films by sweeping to 0.8 V (vs. Ag wire) (Fig. S5). At this stage, Ti is irreversibly oxidized to +4 state with loss of electrochemical activity just as reported by Tang et al.[S2] We have observed that the extinction band red-shifted to 830 nm, but there was no optical shift observed upon cathodic polarization. This again supports the importance of redox nature of the titanium surface towards reversible electrochromic behavior.

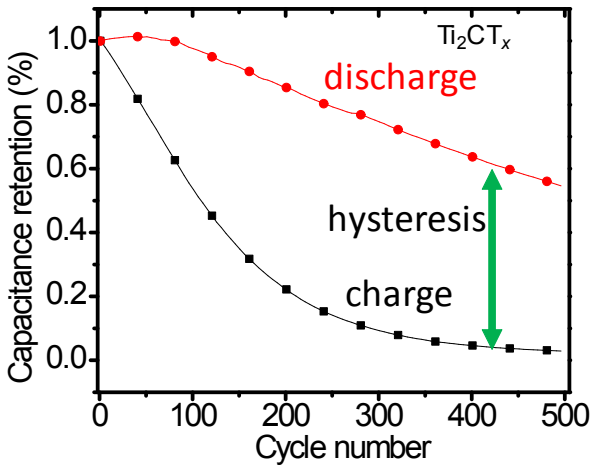

Fig. S6 Charge/discharge capacitance versus cycle number of Ti_2CT_x MXene thin film.

Hysteresis in charge and discharge capacitances with cycle number is an indication for irreversible chemical changes in Ti_2CT_x/ $Ti_{1.6}Nb_{0.4}CT_x$ thin films. Such kind of Behavior is responsible for the cause of increased transmittance with cycle number as shown in Fig. S6.

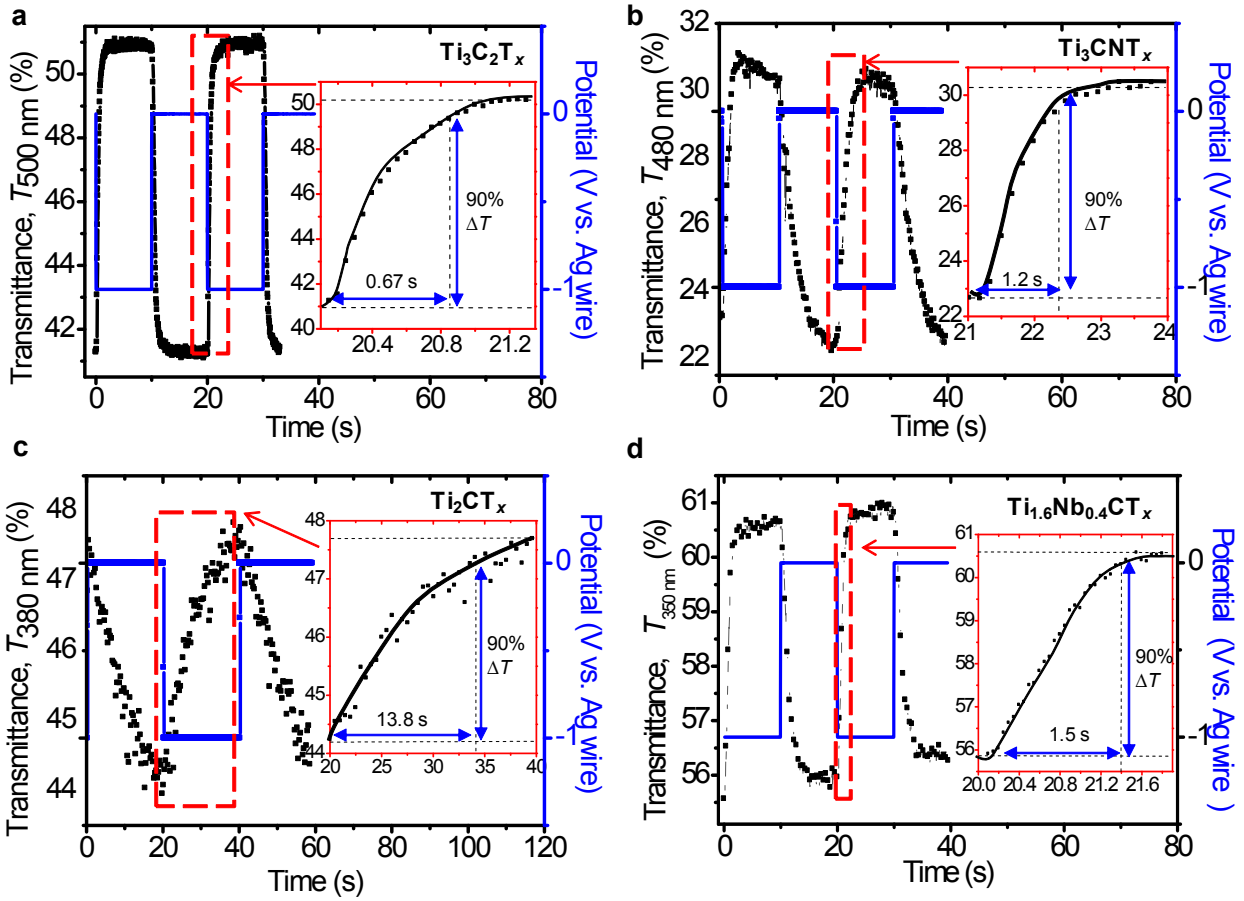

Fig. S7 Transmittance change of MXene electrochromic devices with time under potential pulses between 0 to -1V (vs. Ag wire), (a) $Ti_3C_2T_x$, (b) Ti_3CNT_x, (c) Ti_2CT_x, and (d) $Ti_{1.6}Nb_{0.4}CT_x$. Insets show corresponding switching time estimations for the devices.

Switching time of the electrochromic devices is estimated by measuring the time required to change the transmittance by 90% of ΔT. For the sake of better ionic conductivity and transport, liquid electrolyte (1M H_3PO_4) was chosen over gel electrolytes to study switching times. Switching times of $Ti_3C_2T_x$, Ti_3CNT_x, Ti_2CT_x, and $Ti_{1.6}Nb_{0.4}CT_x$ electrochromic devices are found to be 0.7, 1.2, 14, 1.5 s, respectively (Fig. S5).

Bulk plasma frequency (ω_p), which is proportional to the square root of charge carrier concentration (N_e), is given by

$$\omega_{p^2} = \frac{N_e e^2}{\varepsilon_o m_e} \quad \ldots \text{ equation E2}$$

Where e is elementary charge, ε_o is permittivity of free space, and m_e is the electron effective mass.[S3] Plasmon energy (E_p) is defined as

$$E_p = \hbar\omega_p = h\frac{c}{\lambda_p} \quad \ldots \text{ equation E3}$$

λ_p is the wavelength of plasmon extinction peak, c is speed of light and h is Planck's constant.

Table S1. Summary of optoelectronic and opto-electrochemical performance metrics of MXene thin films with different compositions.

MXenes	**Etching method**	$T_{550\ nm}$ **(%)**	R_s **(Ω/sq)**	**FOM$_e$**	$\Delta\lambda_P$ **(nm)**	ΔT **With extinction peak shift**	**Switching time (s)**	**Areal charge capacitance (mF/cm^2)**	**Increased electron density ΔN_e (cm^{-3})**
$Ti_3C_2T_x$ [S4]	LiF+HCl (MILD)	50	50	17	100	12%	0.64	-	-
$Ti_3C_2T_x$ This work	HF+HCl; LiCl	50	55	7.8	~170	10 %	0.67	3.92	1.07×10^{21}
Ti_3CNT_x This work	LiF+HCl (MILD)	50	200	2.1	-	10 %	1.2	1.87	-
Ti_2CT_x This work	HF+HCl; LiCl	54	5000	0.1	~80	8 %	13.8	1.36	1.18×10^{21}
$Ti_{1.6}Nb_{0.4}CT_x$ This work	LiF+HCl (MILD)	50	400	1	~ 70	6%	1.54	2.21	1.79×10^{21}

Table S2: Comparison of capacitance, switching rates and electrochromic cycling stability (measured at the wavelength where individual MXene has highest transmittance change) of MXene compositions investigated in this study.

Composition	**Capacitance at 20 mV/s (mF/cm^2)**	**Switching time (s)**	**Electrochromic stability (number of cycles to reach 80% of ΔT)**
$Ti_3C_2T_x$	3.92	0.7	2000 (96% ΔT)

Ti_3CNT_x	1.87	1.2	700
Ti_2CT_x	1.36	14	20
$Ti_{1.6}Nb_{0.4}CT_x$	2.21	1.5	300

References

S1 M. Naguib, O. Mashtalir, J. Carle, V. Presser, J. Lu, L. Hultman, Y. Gogotsi and M. W. Barsoum, *ACS Nano*, 2012, **6**, 1322–1331.

S2 J. Tang, T. S. Mathis, N. Kurra, A. Sarycheva, X. Xiao, M. N. Hedhili, Q. Jiang, H. N. Alshareef, B. Xu, F. Pan and Y. Gogotsi, *Angew. Chemie Int. Ed.*, 2019, **58**, 17849–17855.

S3 Y. Zhao, H. Pan, Y. Lou, X. Qiu, J. Zhu and C. Burda, *J. Am. Chem. Soc.*, 2009, **131**, 4253–4261.

S4 P. Salles, E. Quain, N. Kurra, A. Sarycheva and Y. Gogotsi, *Small*, 2018, **14**, 1802864.